Journal of Applied Electrochemistry (2005) 35:177–184
DOI 10.1007/s10800-004-5822-7

Enhanced cyclability of $LiCoO_2$ cathodes coated with alumina derived from carboxylate–alumoxanes

GEORGE TING-KUO FEY[1]*, JIAN-GING CHEN[1] and T. PREM KUMAR[2]
[1]*Department of Chemical and Materials Engineering, National Central University, Chung-Li, Taiwan 32054, R.O.C.*
[2]*Electrochemical Energy Storage Division, Central Electrochemical Research Institute, Karaikudi 630 006, Tamil Nadu, India*
*(*author for correspondence, Tel/fax: +886-3-425-7325, e-mail: gfey@cc.ncu.edu.tw)*

Received 13 October 2004; accepted in revised form 25 October 2004

Key words: Al_2O_3 coating, carboxylate–alumoxanes, coated cathodes, coated $LiCoO_2$, lithium battery

Abstract

$LiCoO_2$ cathodes coated with Al_2O_3 generated from carboxylate–alumoxanes have demonstrated sustainable extended cyclability. The carboxylate–alumoxanes were prepared by reacting boehmite with acetic and substituted acetic acids. TEM images of the coated powders revealed that the coatings were compact and had an average thickness of about 20 nm. XRD data on the coated materials indicated minor changes in the values of the lattice parameters, suggesting the formation of solid solutions of the composition $LiAl_yCo_{1-y}O_2$ on the surface during calcination. ESCA depth profiles of the constituent elements in the coated particles support this theory. *R*-factor values from XRD analysis and galvanostatic cycling studies suggest that a 1.0 wt. % coating formed from a (methoxyethoxy)acetate-alumoxane enhanced the cyclability by a factor of 12. The improved performance is attributed to suppression of the cycle-limiting phase transitions accompanying the charge–discharge processes. Being without environmentally hazardous organic chemicals and by-products, the coating procedure based on carboxylate–alumoxanes is a clean and benign process for industrial exploitation.

1. Introduction

Today's lithium-ion battery technology is based largely on the layered $LiCoO_2$ cathode. $LiCoO_2$, isotypic with α-$NaFeO_2$, has a layered structure in which the Li^+ and Co^{3+} ions occupy alternate (111) planes of a rock salt structure [1]. Lithium can be intercalated and deintercalated reversibly between compositions corresponding to $0.5 < x < 1.0$ in Li_xCoO_2, which limits the charge density to about 140 mAh g^{-1}. The delithiation of $LiCoO_2$ is accompanied by expansion of the host lattice in the *c*-direction, as a result of the increased electrostatic repulsion between adjacent oxygen layers in the lattice [2, 3], and a contraction in the Co–Co distance [4, 5]. Upon repeated cycling, this anisotropic volume change causes structural degradation of the host material [6] and, hence, large capacity fades [7, 8]. The volume changes are ascribed to crystallographic phase transitions occurring in $LiCoO_2$ during charging and discharging at $x < 0.5$ in Li_xCoO_2 [6, 9]. One of the approaches that has been pursued to improve cyclability of the cathode is to coat it with a thin layer of oxide materials such as Al_2O_3 [10–14], B_2O_3 [12], MgO [15, 16], SnO_2 [17], TiO_2 [12, 14] and ZrO_2 [12, 14]. Endo et al. [18] demonstrated the enhanced cycling behavior of $LiCoO_2$ coated with diamond-like carbon obtained by a plasma chemical vapor deposition technique. The improved cycling performance of the coated materials is believed to result from structural stability brought about by substitutional oxides formed on the cathode surface [10, 11, 15–17], as well as by the suppression of cycle-limiting phase transitions during the intercalation–deintercalation processes by high fracture-tough coating materials [12].

Al_2O_3, as a coating material to improve the cyclability of $LiCoO_2$, has been investigated by several groups [9–13]. The precursors used have generally been expensive alkoxide precursors such as aluminum *sec*-butoxide and aluminum ethylhexanate diisopropoxide, which make them questionable for commercial applications. Furthermore, the green bodies of the coating material are generated by a sol–gel procedure in organic solvents like *iso*-propanol. The release of the solvent and alcoholic by-products formed by hydrolysis of the alkoxide during such coating processes can pose an environmental hazard.

Recently, we demonstrated a simple, economic mechano-thermal process for coating cathode materials with pre-formed nanoparticulates of silica [19], pseudo-boehmite [20], and boehmite [21]. An attractive feature of this process was that it employed environmentally benign chemicals for the coating

procedure. In this paper, we present the results of our study on commercial $LiCoO_2$ coated with Al_2O_3 derived from environmentally benign carboxylate–alumoxanes.

2. Experimental

Carboxylate–alumoxane precursors were prepared according to procedures described by Callender et al. [22]. A commercial sample of boehmite, $[Al(O)(OH)]_n$ (Catapal B, average particle size: 60 μm; BET surface area: 240 $m^2\ g^{-1}$), was used. The carboxylic acids used were acetic acid [CH_3COOH], methoxyacetic acid [CH_3OCH_2COOH], (methoxyethoxy)acetic acid [CH_3O-$CH_2CH_2OCH_2COOH$], and [(methoxyethoxy)ethoxy]-acetic acid [$CH_3O(CH_2CH_2O)_2CH_2COOH$]. The acids are abbreviated in the text as A, MA, MEA and MEEA, respectively. The carboxylate–alumoxanes synthesized were redispersed in water, and sonicated with a commercial sample of $LiCoO_2$ (Coremax Taiwan Corporation), such that the weight ratio of $LiCoO_2$ to Al_2O_3 (formed upon calcination) was 99:1. A subsequent slow evaporation of water at 50 °C resulted in a white dry mass of the carboxylate–alumoxane-coated $LiCoO_2$ particles. This was followed by calcination at 450 °C for 10 h, when the carboxylate–alumoxane decomposed to yield an adherent coating of Al_2O_3 on the particles.

Thermogravimetric and differential thermal analyses of the carboxylate–alumoxanes were carried out on a Seiko SSC-5000 TG/DTA/DSC/TMA analyzer at a heating ramp of 10 °C min^{-1} in air. The typical sample weight was 10 mg. An X-ray diffractometer (Siemens D-5000, Mac Science MXP18) equipped with a nickel-filtered Cu-K_α radiation source was used for structural analysis. The diffraction patterns were recorded between scattering angles of 5° and 80° in steps of 0.05°. BET surface area measurements were carried out on a Micromeritics ASAP 2010 surface area analyzer. The microstructures of the coated particles were examined by a JEOL JEM-200FXII transmission electron microscope equipped with a LaB_6 gun. The samples for TEM studies were prepared by dispersing the coated powders in ethanol, placing a drop of the clear solution on a carbon-coated copper grid, and subsequent drying. Depth profiles of aluminum, cobalt and oxygen in the coated materials were recorded by ESCA (VG Scientific Escalab 250) in order to analyze the spatial distribution of the ions in the cathode particles.

Coin cells of the 2032 configuration were assembled in an argon-filled VAC MO40-1 glove box in which the oxygen and water contents were maintained below 2 ppm. Lithium metal (Foote Mineral) was used as the anode and a 1 M solution of $LiPF_6$ in EC:DEC (1:1 v/v) (Tomiyama Chemicals) was used as the electrolyte. The cathode was prepared by blade-coating a slurry of 85 wt. % coated active material with 10 wt. % conductive carbon black and 5 wt. % poly(vinylidene fluoride) binder in *N*-methyl-2-pyrrolidone on an aluminum foil, drying overnight at 120 °C in an oven, roller-pressing the dried coated foil, and punching out circular discs. The cells were cycled at a 0.2 C rate (with respect to a theoretical capacity of 274 mAh g^{-1}) between 2.75 and 4.40 V in a multichannel battery tester (Maccor 4000). Phase transitions occurring during the cycling processes were examined by slow scan cyclic voltammetry, performed with a three-electrode glass cell. The working electrodes were prepared with the cathode powders as described above, but coated on both sides of the aluminum foil. The cells for the cyclic voltammetric studies were assembled inside the glove box with lithium metal foil serving as both counter and reference electrodes. The electrolyte used was the same as that for the coin cell. Cyclic voltammograms were run on a Solartron 1287 Electrochemical Interface at a scan rate of 0.1 mV s^{-1} between 3.0 and 4.4 V.

3. Results and discussion

3.1. *Thermolysis of carboxylate–alumoxanes*

Carboxylate–alumoxanes, represented by the general formula $[Al(O)_x(OH)_y(OOCR)_z]_n$, are formed when the mineral boehmite, $[AlO(OH)]_n$, reacts with a carboxylic acid according to the reaction [22, 23]

$$[Al(O)(OH)]_n + nz\,RCOOH \rightarrow [Al(O)_x(OH)_y(OOCR)_z]_n$$

The products have an alumina core surrounded by covalently bonded carboxylate moieties. The carboxylate ions 'unzip' the boehmite structure, abstract, and stabilize nanoparticulate fragments of boehmite by replacing its oxide and hydroxide groups with acid groups [22–24]. Thermolysis of carboxylate–alumoxanes yields alumina [24, 25]. The nature of the carboxylate–alumoxanes depends on the identity of the carboxylic acid used [22]. Thus, we should expect the characteristics of the alumina product to be dependent on the precursor. The thermograms, differential thermograms and differential thermal analytical curves recorded with the different carboxylate–alumoxanes are presented in Figure 1. The alumoxanes decomposed in a two-step exothermic process to yield alumina. It is clear that between 450 and 800 °C no further changes occur to the product. In fact, it was shown [24] that in the case of carboxylate–alumoxanes such as MEEA–alumoxane the initial product of decomposition was γ-Al_2O_3, which transformed to α-Al_2O_3 at temperatures above 1000 °C.

Because Al_2O_3 is generated from an aqueous solution of the carboxylate–alumoxane in which the $LiCoO_2$ powder is stirred, the product can be expected to lodge itself in the micro-crevices of the cathode particles. The intimate contact between the alumina particles and the core surface, and the subsequent calcination should result in thin, compact and adherent coatings.

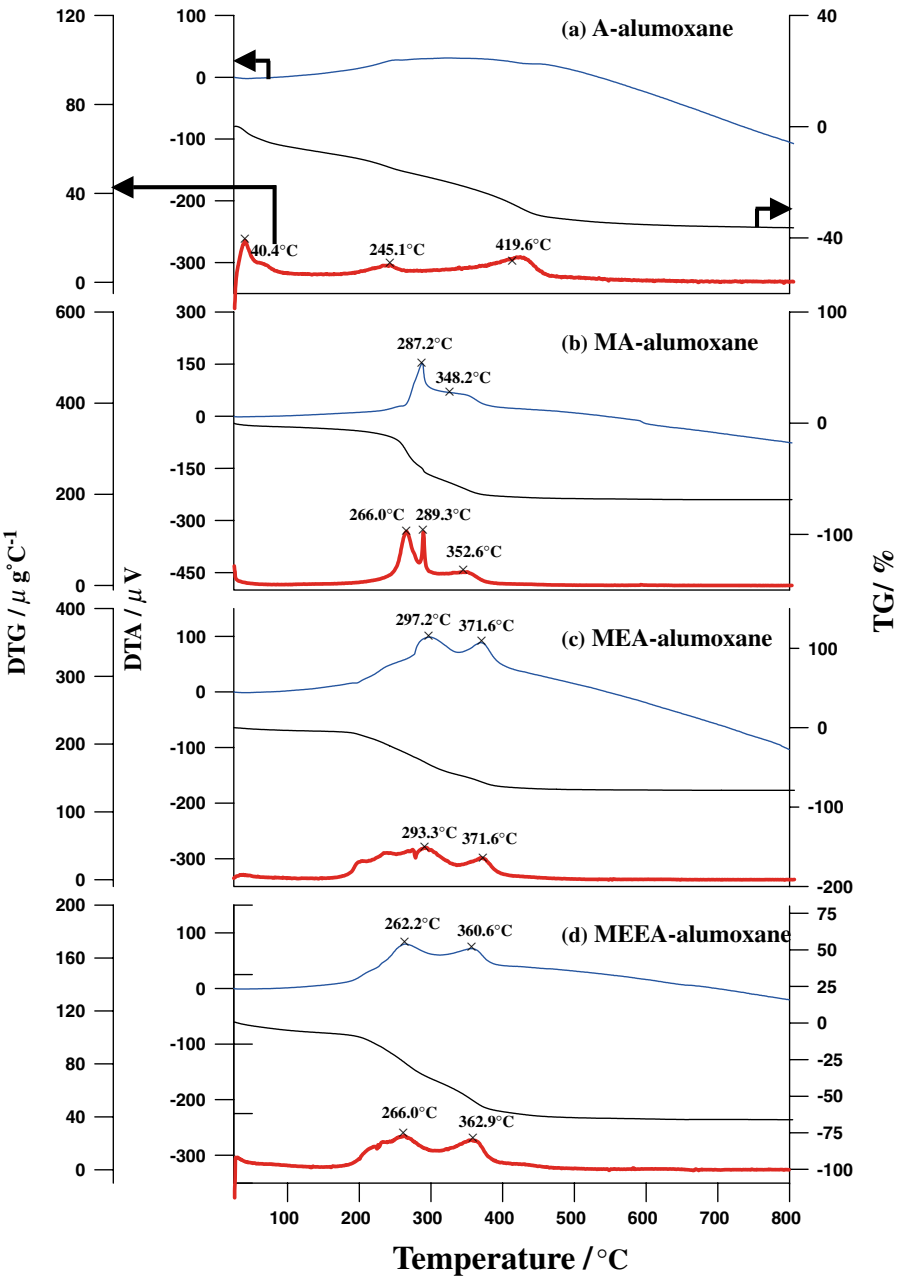

Fig. 1. TG and DTA curves recorded with the various carboxylate alumoxanes.

3.2. *X-ray diffraction*

The X-ray diffraction pattern of the product obtained by the decomposition of A–alumoxane at 450 °C is shown in Figure 2a. A comparison with the JCPDS pattern (Figure 2b) confirms that the product was α-Al_2O_3. However, the products obtained in the other cases were γ-Al_2O_3, as shown, for example, by the X-ray diffraction pattern of the product obtained from MEA–alumoxane (Figure 3a).

Figure 4 shows the X-ray diffraction patterns of the bare $LiCoO_2$ and Al_2O_3-coated $LiCoO_2$ powders. The reflections of all the materials conform to the $R\bar{3}m$ symmetry of the core material. The absence of diffraction patterns corresponding to Al_2O_3 shows that the coating material exists as a thin film and possibly as a substitutional oxide formed by interaction with the underlying $LiCoO_2$. As Table 1 shows, the lattice constants a and c of the coated materials differ from those of the bare cathode material, suggesting the presence of solid solutions formed by the reaction of the Al_2O_3 particles with the core $LiCoO_2$. It is conceivable that during the 10-h calcination process, substitutional compounds of the composition $LiAl_yCo_{1-y}O_2$ could have formed through solid-phase reactions between the two oxidic phases. Several groups have proposed the formation of such inter-oxide surface compositions [10, 16, 17, 26].

The I_{003}/I_{104} intensity ratios of all the coated materials (Table 1) were higher than 1, and were generally higher than the ratio for the bare $LiCoO_2$, which indicates that the samples had good cation ordering [27], also evident

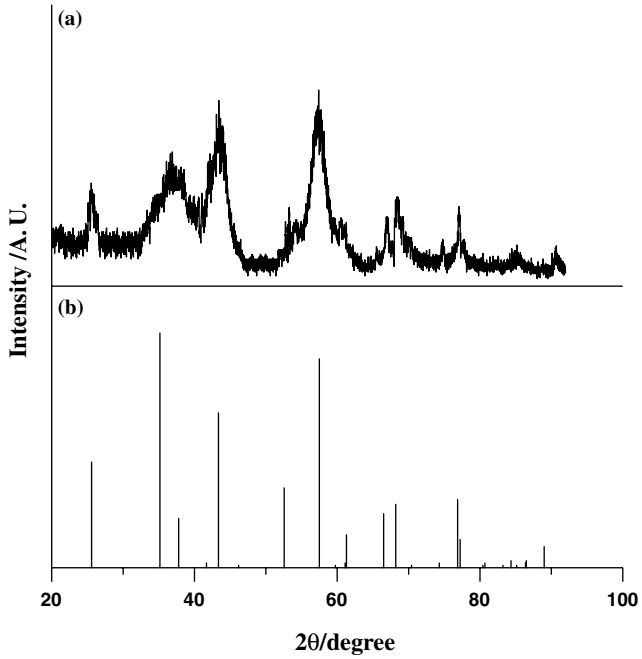

Fig. 2. X-ray diffraction patterns of (a) the decomposition product of A–alumoxane; and (b) α-Al_2O_3 (JCPDS).

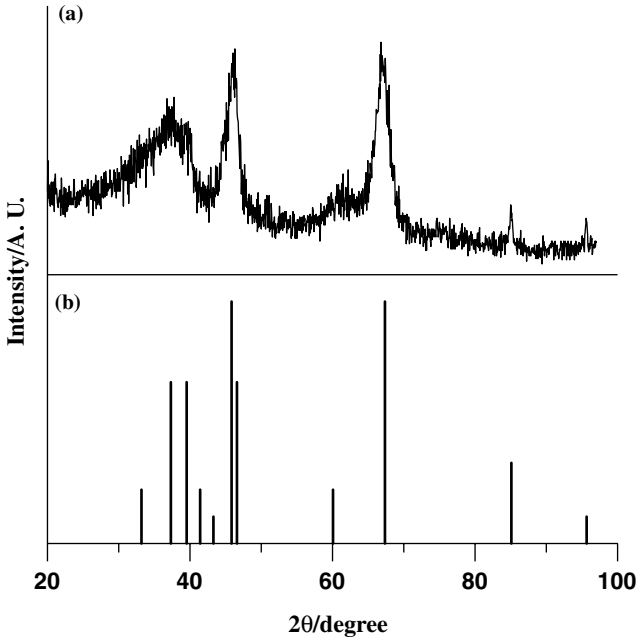

Fig. 3. X-ray diffraction patterns of (a) the decomposition product of MEA–alumoxane; and (b) γ-Al_2O_3 (JCPDS).

from the well-separated (108) and (110) reflections [27, 28]. According to Dahn et al. [29, 30], the *R*-factor, defined as the ratio of the intensities of the hexagonal characteristic doublet peaks (006) and (102) to the (101) peak, is an indicator of hexagonal ordering. According to those authors [29, 30], the lower the *R*-factor, the better the hexagonal ordering and, hence, the electrochemical performance. While the value of the *R*-factor for the bare $LiCoO_2$ was 0.77, the *R*-factors for the materials coated with Al_2O_3 obtained from A–alumoxane, MA–alumoxane, MEA–alumoxane and MEEA–alumoxane were 0.43, 0.45, 0.41 and 0.50, respectively (Table 1). It can be seen that the *R*-factor values for the coated samples were generally smaller than for the bare sample. As will be shown below, the electrochemical behavior of the coated samples closely follows this trend in *R*-factor.

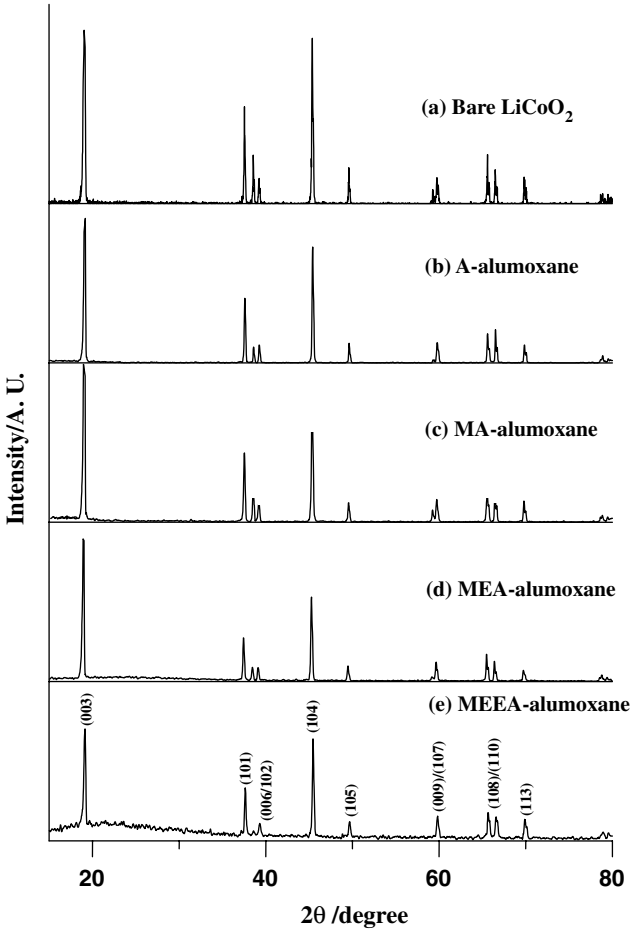

Fig. 4. X-ray diffraction patterns of (a) the bare and (b–e) Al_2O_3-coated $LiCoO_2$ powders. Precursors: (b) A–alumoxane; (c) MA–alumoxane; (d) MEA–alumoxane; and (e) MEEA–alumoxane.

Table 1. XRD data on the bare and Al_2O_3-coated $LiCoO_2$

Sample coating	Unit cell volume					*R*-factor
	a(Å)	c(Å)	(c/a)	(I_{003}/I_{104})	Å^3	
Bare $LiCoO_2$	2.830	14.001	4.95	1.86	98.0	0.77
A–alumoxane	2.809	13.928	4.96	2.26	95.2	0.43
MA–alumoxane	2.804	13.967	4.98	2.03	95.1	0.45
MEA–alumoxane	2.814	14.030	4.99	2.10	96.2	0.41
MEEA–alumoxane	2.807	13.900	4.95	1.10	94.8	0.50

3.3. *Morphology*

Figure 5 is a representative TEM image of $LiCoO_2$ coated with Al_2O_3 (1.0 wt %) obtained from MEA–alumoxane. The alumina coating formed a

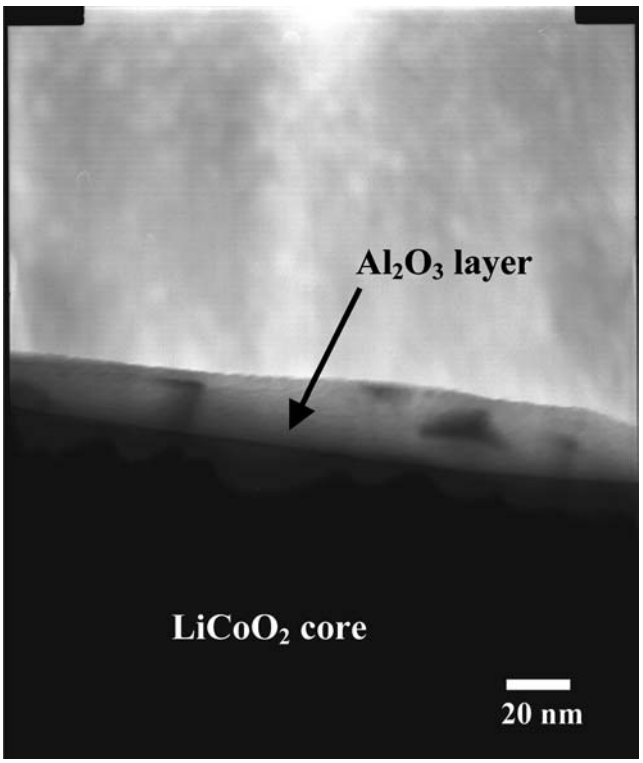

Fig. 5. TEM image of an $LiCoO_2$ particle coated with Al_2O_3 (1.0 wt. %). Precursor: MEA–alumoxane.

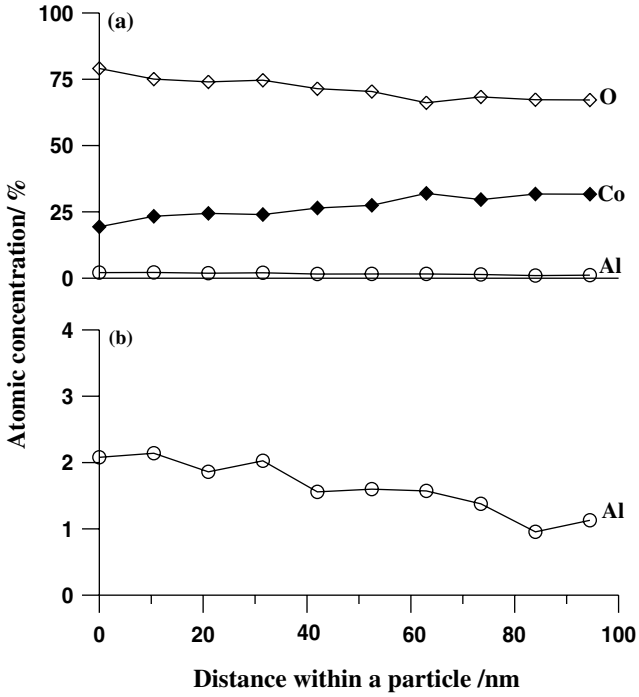

Fig. 6. (a) ESCA depth profiles of an $LiCoO_2$ particle coated with 1.0 wt % Al_2O_3. Precursor: MEA–alumoxane. (b) Expanded depth profile of aluminum in the above.

uniform and compact kernel (light region) over the $LiCoO_2$ particle (dark region). Typical thickness of the kernel was around 20 nm, which agrees with the results of our ESCA depth profile analysis.

The BET surface areas of the bare and the coated powders (1.0 wt %, MEA–alumoxane) were 0.62 and 1.30 $m^2\ g^{-1}$, respectively. The increased surface area of the cathode material may be from the greater surface area of the alumina generated by the decomposition of the carboxylate–alumoxanes. During calcination, a major part of the coating may be consumed in generating the inter-oxide surface compositions. The compactness of the kernel, as observed from our TEM examination (Figure 5), lends credence to this reasoning.

3.4. *ESCA*

The spatial distribution of the constituent elements in the alumina-coated $LiCoO_2$ (precursor: MEA–alumoxane) is displayed in the depth profiles presented in Figure 6a. The concentration of cobalt increased to a depth of about 60 nm and then leveled off. The small concentration of cobalt observed on the surface suggests that cobalt ions from the core of the particles diffuse into the alumina layer during the calcination process. While, the inter-diffusion would alter the composition of the $LiCoO_2$ core, our XRD results do not show any significant structural changes that may accompany this ionic diffusion. The concentration of aluminum was small, typically less than the 2 at.%. Some aluminum seems to have penetrated deep into the bulk of the cathode particles during the calcination process (Figure 6b), as supported by our XRD results, which suggested the formation of substitutional surface oxides. However, the identity of these surface oxides can be determined by solid state Al-NMR analysis, which is currently under way.

3.5. *Galvanostatic cycling*

The effectiveness of the Al_2O_3 coating on the cyclability of the cathode material was studied by galvanostatic cycling. First, the effect of calcination was investigated. For this, bare $LiCoO_2$, $LiCoO_2$ coated with the green coating (undecomposed A–alumoxane, 1.0 wt %), and $LiCoO_2$ coated with Al_2O_3 (A–alumoxane, 1.0 wt %, calcined for 10 h at 450 °C) were used. Figure 7 illustrates the effect of calcination on the electrochemical characteristics of the coated $LiCoO_2$ material. While the first-cycle discharge capacity of the bare $LiCoO_2$ sample was 167 mAh g^{-1}, the capacities of the materials with the green and calcined coatings were 133 and 161 mAh g^{-1}, respectively. Although the capacity of the green (uncalcined) coated material rose to 140 mAh g^{-1} in the second cycle, it faded rapidly. For a cut-off value of 80% for the capacity retention, calculated with the first-cycle discharge capacity of the bare material as the reference, the number of cycles that the bare $LiCoO_2$ could sustain was 14, while those sustained by $LiCoO_2$ with the green and calcined coatings were 17 and 132, respectively. Thus, it is clear that calcination is an important step because it not only generates an *in situ* coating of alumina, but also helps

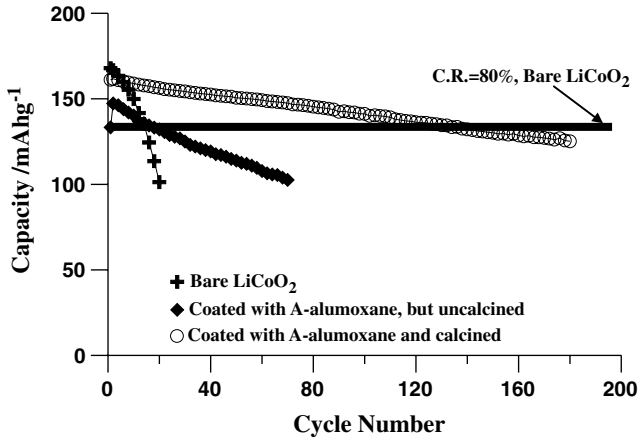

Fig. 7. Cycling performance of (a) bare $LiCoO_2$; (b) $LiCoO_2$ coated with A–alumoxane, but uncalcined; and (c) $LiCoO_2$ coated with A–alumoxane and calcined.

form a compact kernel of substitutional oxides on the cathode particles during the subsequent calcination step.

The cycling behavior of $LiCoO_2$ coated with 1.0 wt % Al_2O_3 derived from boehmite and pseudo-boehmite-based carboxylate–alumoxanes are presented in Figure 8. The first-cycle capacities for the coated samples were 161, 162, 159 and 163 mAh g^{-1}, respectively, for A–alumoxane, MA–alumoxane, MEA–alumoxane, and MEEA–alumoxane. The lower capacities compared to the bare sample (168 mAh g^{-1}) are attributed to the presence of the electro-inactive alumina and/or to the lesser number of Co^{3+} ions available in the substituted surface oxide. The cycling behavior of the coated samples shows that the MEA–alumoxane gave the best results, sustaining 167 cycles, respectively, before they reached the 80% capacity cut-off based on their respective first-cycle capacities. Thus, it can be seen that the coatings improved the cyclability of the core $LiCoO_2$ material as much as 12 times.

It is likely that the properties of the coatings would depend on the complexing acids because the ratio of the surface coverage of the alumoxane molecule to its

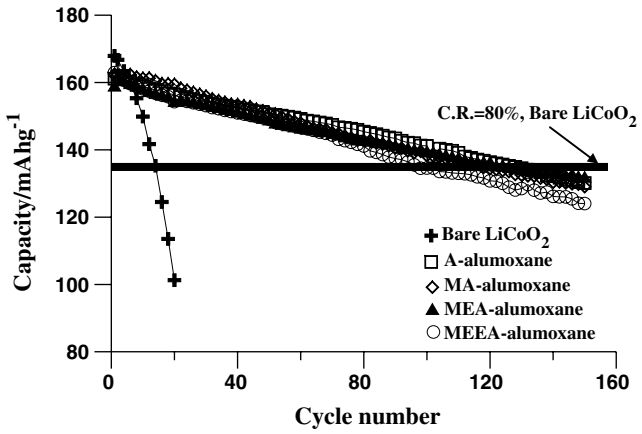

Fig. 8. Cycling behavior of $LiCoO_2$ coated with carboxylate–alumoxane-derived Al_2O_3. Coating level: 1.0 wt %.

length would decrease as we proceed from the acetate–alumoxane to the higher order carboxylate–alumoxanes. For this reason, the particles formed from the lower order alumoxanes should be closer to one another than those obtained from the higher order alumoxanes. However, the energy released in the thermolysis process, which will be higher for the higher order alumoxanes, can influence the compactness of the resultant coating and even the particles that comprise it. The larger amount of heat energy generated by the combustion of the higher order alumoxanes can lead to greater inter-diffusion of ions between the core and the coating materials, providing more compact kernels. At the same time, the greater heat energy can produce highly sintered particles, which can influence the compactness of the coating. However, the product obtained from the acetate–alumoxane was α-Al_2O_3 while that from the other alumoxanes was γ-Al_2O_3. Thus, the phase of the coating material, its compactness, and the size of the particles that comprise it will determine the effectiveness of the coating.

The beneficial effect of doping $LiCoO_2$ with aluminum is well documented [31–35]. Aluminum incorporation suppresses anisotropic structural changes in the cathode material by helping maintain inter-layer distances [36]. Jang et al. [37] proposed that the fixed valency of aluminum forces a greater exchange of electrons with the lattice oxygen, increasing the lithium intercalation voltages [32, 38]. Aluminum doping has also been shown to contribute to good discharge capacity as well as improved stability based on less electrolyte decomposition [39]. In the present study, any doping with aluminum can be expected only on the surface as indicated by the variations in the X-ray diffraction patterns. In fact, the cyclability of the materials is generally commensurate with the trend in the variation of the *R*-factor. Thus, it can be seen from Table 1 that the bare material with an *R*-factor value of 0.77 sustained only 14 cycles, while the *R*-factor values of the alumina-coated materials derived from boehmite–A, boehmite–MA, boehmite–MEA and boehmite–MEEA and their respective cycle-lifes were 0.43 (135), 0.45 (159), 0.41 (184) and 0.50 (100). The cyclability reached a maximum for the coating derived from the (methoxyethoxy)acetate–alumoxane.

Thus, the coating process presented here results in cathode-active materials with improved cyclability. The process is attractive for a number of reasons: (1) the use of the commercially available mineral boehmite and alkoxy-substituted acetic acids, which have a cost advantage over the expensive alkoxide precursors used in sol–gel coatings; (2) the infinite stability, both as a solid and as an aqueous solution, of the nanoparticulate carboxylate–alumoxane precursors (as compared to moisture-sensitive sol–gel precursors); (3) aqueous solution processing; and (4) absence of environmentally hazardous vapors during processing, especially

during calcination of green bodies of the coating material.

3.6. *Cyclic voltammetry*

$LiCoO_2$ cathodes are known to undergo a hexagonal–monoclinic–hexagonal phase transition above 4.1 V vs. Li^+/Li, which leads to capacity fade upon repeated cycling [6–8]. This phase transition is accompanied by a 1.2% expansion of the lattice in the *c*-direction, which is considered to be above the limit of ~0.1% in elastic strain that oxides can tolerate [40]. The abrupt shrinkage of the *c*-axis, which accounts for about 9% in volume change [41], can induce cracks in the particles, reducing the cyclability [6]. According to Kavan and Gratzel [42], cyclic voltammetry is sensitive to phase transformations occurring during electrochemical reactions. Thus, slow scan cyclic voltammetry was performed in order to examine the effect of the coating on the phase transitions that accompany the charge–discharge processes. Figure 9a presents the cyclic voltammograms of the bare $LiCoO_2$, while Figure 9b presents those for $LiCoO_2$ coated with Al_2O_3 derived from A–alumoxane. The major peaks centering around 3.95 and 3.85 V in the cyclic voltammograms correspond to the oxidation of Co^{3+} ion to Co^{4+} accompanying delithiation and the reduction of Co^{4+} to Co^{3+} accompanying the lithiation processes, respectively. The minor ones are associated with phase changes. As indicated in the figures, the originally hexagonal structure of the host lattice transforms into a monoclinic structure and then reverts to the hexagonal structure as delithiation proceeds. The reverse sequence of phase changes is seen during lithiation. It can be seen from the cyclic voltammograms of the bare $LiCoO_2$ that the peaks corresponding to the hexagonal–monoclinic–hexagonal phase transitions persisted upon cycling. However, the peaks corresponding to the phase changes appeared only in the first sweep in the case of the coated material. From the second sweep onwards, these peaks were conspicuously absent, which shows that any defect in the coating that might have been present initially was repaired upon cycling. The presence of cracks, pinholes, and other coating defects on coated surfaces is inevitable. However, such defects may form and close with the application of a load, or upon thermal cycling. In our case, changes in the surface texture that occurred as a result of the contraction and expansion of the lattice during the cycling process may have enabled the particles of the coating material to become ingrained in the crevices and cracks on the cathode surface. The more compact kernel that resulted led to a suppression of the phase transitions, enhancing the cyclability of the coated material. The absence of phase transitions in the coated samples ensures negligible strain, resulting in its longevity.

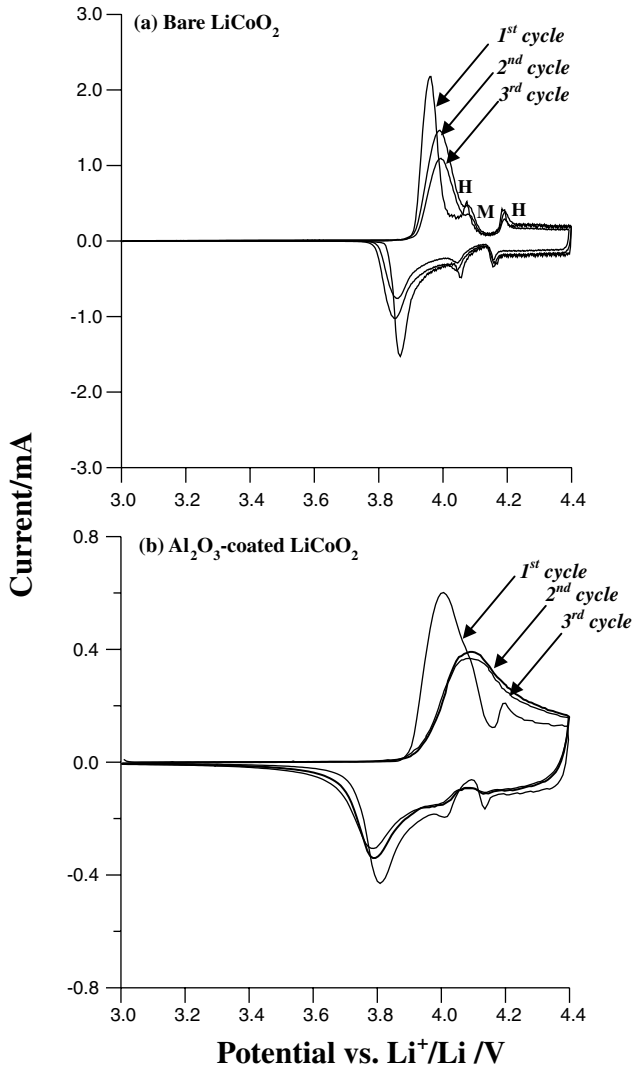

Fig. 9. Cyclic voltammograms of (a) bare $LiCoO_2$ and (b) $LiCoO_2$ coated with Al_2O_3. Precursor: MEA–alumoxane.

4. Conclusions

Carboxylate–alumoxanes were used as precursors for coating commercial $LiCoO_2$ cathode samples with Al_2O_3. Although the XRD patterns of the coated materials did not show any extraneous peaks corresponding to the coated particles, the slight variations in the values of the lattice parameters of the coated samples suggest that upon calcination the coated alumina particles formed a substitutional compound of the type $LiAl_yCo_{1-y}O_2$ on the surface. TEM images showed that the particles were covered with a compact, adherent kernel. ESCA depth profiles indicated that small amounts of aluminum diffused into the bulk of cathode material during the calcination process, possibly in the form of inter-oxide compositions. Cycling studies showed that a 12-fold improvement in the cyclability of $LiCoO_2$ was achieved by Al_2O_3 coating from MEA–alumoxane. The lowest *R*-factor value of this coated material indicates that good structural stability contributed to its high cyclability. In addition

to its simplicity, this process employs no hazardous organic solvents, which makes it viable for commercial exploitation.

Acknowledgements

Financial support for this work was provided by the National Science Council of the Republic of China under contract No. NSC-91-2622-E-008-006-CC3. TPK thanks the NSC for the award of a post-doctoral fellowship.

References

1. L.D. Dyer, B.S. Borie Jr. and G.P. Smith, *J. Am. Chem. Soc.* **76** (1954) 1499.
2. K. Mizushima, P.C. Jones, P.J. Wiseman and J.B. Goodenough, *Mater. Res. Bull.* **15** (1980) 783.
3. J.B. Goodenough, K. Mizushima and T. Takeda, *Jpn. J. Appl. Phys.* **19** (1980) 305.
4. J.N. Reimers and J.R. Dahn, *J. Electrochem. Soc.* **139** (1992) 2091.
5. T. Ohzuku and A. Ueda, *J. Electrochem. Soc.* **141** (1994) 2972.
6. H.F. Wang, Y.I. Jang, B.Y. Huang, D.R. Sadoway and Y.M. Chiang, *J. Electrochem. Soc.* **146** (1999) 473.
7. E. Plichita, S. Slane, M. Uchiyama, M. Salomon, D. Chua, W.B. Ebner and H.W. Lin, *J. Electrochem. Soc.* **136** (1989) 1865.
8. G.G. Amatucci, J.M. Tarascon and L.C. Klein, *Solid State Ion.* **83** (1996) 167.
9. S. Lavasseur, M. Menetrier, E. Suard and C. Delmas, *Solid State Ion.* **128** (2000) 11.
10. J. Cho, Y.J. Kim and B. Park, *Chem. Mater.* **12** (2000) 3788.
11. J. Cho, Y.J. Kim and B. Park, *J. Electrochem. Soc.* **148** (2001) A1110.
12. J. Cho, Y.J. Kim, T.-J. Kim and B. Park, *Angew. Chem. Int. Ed.* **40** (2001) 3367.
13. L. Liu, Z. Wang, H. Li, L. Chen and X. Huang, *Solid State Ion.* **152–153** (2002) 341.
14. A.M. Kannan, L. Rabenberg and A. Manthiram, *Electrochem. Solid-State Lett.* **6** (2003) A16.
15. M. Mladenov, R. Stoyanova, E. Zhecheva and S. Vassilev, *Electrochem. Commun.* **3** (2001) 410.
16. Z. Wang, C. Wu, L. Liu, F. Wu, L. Chen and X. Huang, *J. Electrochem. Soc.* **149** (2002) A466.
17. J. Cho, C.-S. Kim and S.-I. Yoo, *Electrochem. Solid-State Lett.* **3** (2000) 362.
18. E. Endo, T. Yasuda, A. Kita, K. Yamamura and K. Sekai, *J. Electrochem. Soc.* **147** (2000) 1291.
19. G.T.K. Fey, H.Z. Yang, T.P. Kumar, S.P. Naik, A.S.T. Chiang, D.C. Lee and J.R. Lin, *J. Power Sources* **132** (2004) 172.
20. G.T.K. Fey, Z.X. Weng, J.G. Chen, C.Z. Lu, T.P. Kumar, S.P. Naik and A.S.T. Chiang, *Mater. Lett.* (Communicated).
21. G.T.K. Fey, Z.X. Weng, J.G. Chen, C.Z. Lu, T.P. Kumar, S.P. Naik and A.S.T. Chiang, D.C. Lee and J.R. Lin, *J. Appl. Electrochem.* **34** (2004) 715.
22. R.L. Callender, C.J. Harlan, N.M. Shapiro, C.D. Jones, D.L. Callahan, M.R. Wiesner, D.B. MacQueen, R. Cook and A.R. Barron, *Chem. Mater.* **9** (1997) 2418.
23. C.C. Landry, N. Pappe, M.R. Mason, A.W. Apblett, A.N. Tyler, A.N. MacInnes and A.R. Barron, *J. Mater. Chem.* **5** (1995) 331.
24. R.L. Callender and A.R. Barron, *Adv. Mater.* **12** (2000) 734.
25. C.J. Harlan, A. Kareiva, D.B. MacQueen, R. Cook and A.R. Barron, *Adv. Mater.* 9 (1997) 68.
26. H.J. Kweon, S.J. Kim and D.G. Park, *J. Power Sources* **88** (2000) 255.
27. J. Kim, P. Fulmer and A. Manthiram, *Mater. Res. Bull.* **34** (1999) 571.
28. R.J. Gummow, M.M. Thackeray, W.I.F. David and S. Hull, *Mater. Res. Bull.* **27** (1992) 327.
29. J.N. Reimers, E. Rossen, C.D. Jones and J.R. Dahn, *Solid State Ion.* **61** (1993) 335.
30. J.R. Dahn, U. von Sacken and C.A. Michel, *Solid State Ion.* **44** (1990) 87.
31. S.-T. Myung, N. Kumagai, S. Komaba and H.-T. Chung, *Solid State Ion.* **139** (2001) 47.
32. G. Ceder, Y.-M. Chiang, D.R. Sadoway, M.K. Aydinol, Y.-I. Jang and B. Huang, *Nature* **392** (1998) 694.
33. Y.-I. Jang, B. Huang, H. Wang, G.R. Maskaly, G. Ceder, D.R. Sadoway, Y.-M. Chiang, H. Liu and H. Tamura, *J. Power Sources* **81–82** (1999) 589.
34. W.S. Yoon, K.K. Lee and K.B. Kim, *J. Power Sources* **97–98** (2001) 303.
35. S. Castro-Garcia, A. Castro-Couceiro, M.A. Senaris-Rodriguez, F. Soulette and C. Julien, *Solid State Ion.* **156** (2003) 15.
36. T. Ohzuku, A. Ueda and M. Kouguchi, *J. Electrochem. Soc.* **142** (1995) 4033.
37. Y.-I. Jang, B. Huang, H. Wang, D.R. Sadoway, G. Ceder, Y.-M. Chiang, H. Liu and H. Tamura, *J. Electrochem. Soc.* **146** (1999) 862.
38. M.K. Aydinol, A.K. Kohan, G. Ceder, K. Cho and J. Joanopoulos, *Phys. Rev.* **B 56** (1997) 1354.
39. G.A. Nazri, A. Rougier and K.F. Kia, *Mater. Res. Soc. Symp. Proc.* **435** (1997) 635.
40. L.H. van Vlack, 'Physical Ceramics for Engineers', (Addison-Wesley Publishing, Reading, MA, 1964).
41. K. Dokko, M. Nishizawa, S. Horikoshi, T. Itoh, M. Mohamedi and I. Uchida, *Electrochem. Solid-State Lett.* **3** (2000) 125.
42. L. Kavan and M. Gratzel, *Electrochem. Solid-State Lett.* **5** (2002) A39.